Available online at www.sciencedirect.com
ScienceDirect
Thermochimica Acta 448 (2006) 136–146
thermochimica acta
www.elsevier.com/locate/tca

Reversible melting of high molar mass poly(oxyethylene)☆

Wulin Qiu [a,b], Bernhard Wunderlich [a,b,*]

[a] Department of Chemistry, The University of Tennessee, Knoxville, TN 37996-1600, United States
[b] Chemical Sciences Division, Oak Ridge National Laboratory, Oak Ridge, TN 37831-6197, United States

Received 25 May 2006; received in revised form 8 July 2006; accepted 17 July 2006
Available online 25 July 2006

Abstract

The heat capacity, C_p, of poly(oxyethylene), POE, with a molar mass of 900,000 Da, was analyzed by temperature-modulated differential scanning calorimetry, TMDSC. The high molar mass POE crystals are in a folded-chain macroconformation and show some locally reversible melting, starting already at about 250 K. At 335 K the thermodynamic heat capacity reaches the level of the melt. The end of melting of a high-crystallinity sample was analyzed quasi-isothermally with varying modulation amplitudes from 0.2 to 3.0 K to study the reversible crystallinity. A new internal calibration method was developed which allows to quantitatively assess small fractions of reversibly melting crystals in the presence of the reversible heat capacity and large amounts of irreversible melting. The specific reversibility decreases to small values in the vicinity of the end of melting, but does not seem to go to zero. The reversible melting is close to symmetric with a small fraction crystallizing slower than melting, i.e., under the chosen condition some of the melting and crystallization remains reversing. The collected data behave as one expects for a crystallization governed by molecular nucleation and not as one would expect from the formation of an intermediate mesophase on crystallization. The method developed allows a study of the active surface of melting and crystallization of flexible macromolecules.
Published by Elsevier B.V.

Keywords: Crystal; Glass transition; Poly(oxyethylene); Reversible melting; Temperature-modulated differential scanning calorimetry (TMDSC)

1. Introduction

Poly(oxyethylene), POE $[O–(CH_2–)_2]_x$, is a structurally well characterized, semicrystalline, flexible macromolecule [1–14]. Earlier, thermal analyses identified the glass transition temperatures, T_g, for the amorphous [15], semicrystalline [16], and crystalline state [17,18], and the melting temperatures, T_m, and heats of fusion, H_f [19]. The integral thermodynamic functions, H, S, and G, were derived from the heat capacity, C_p, and evaluated for the equilibrium states [20]. The thermal properties, in turn, were linked to the molecular motion [21]. All these quantities have been established and compared to other polymers in the framework of the ATHAS Data Bank [22,23].

The symbol C_p for heat capacity is applied in this paper to the thermodynamic as well as the apparent, reversing, and total heat capacities, all measured at constant pressure. In case the discussed C_p needs to be distinguished from the others, the appropriate adjective is added. The term apparent, thermodynamic C_p applies to a heat capacity that includes latent heat effects, as expressed by the equation for the change in overall enthalpy:

$$\mathrm{d}H = \left(\frac{\partial H}{\partial T}\right)_{p,n} \mathrm{d}T + \left(\frac{\partial H}{\partial n}\right)_{p,T} \mathrm{d}n, \quad (1)$$

where $(\partial H/\partial T)_{p,n}$ represents the thermodynamic heat capacity, the latent heat effect is $(\partial H/\partial n)_{p,T}$, and d$T$ and dn the changes in temperature and composition, respectively. For crystallization and melting, the composition can be represented by the crystallinity, w_c, with the latent heat being the heat of fusion, ΔH_f. The apparent heat capacity is dH/dT, and the changes in composition during dT must be evaluated separately from $(\partial H/\partial n)_{p,T}/(\mathrm{d}n/\mathrm{d}T)$, or $(\partial \Delta H_f/\partial w_c)_{p,T}/(\mathrm{d}w_c/\mathrm{d}T)$.

The term "reversing" is used for the apparent C_p, deconvoluted from the "non-reversing" C_p by subtracting the "total" C_p which refers to the sliding average over one modulation

☆ This article has been authored by a contractor of the U.S. Government under the contract no. DOE-AC05-00OR22725. Accordingly, the U.S. Government retains a non-exclusive, royalty-free license to publish, or reproduce the published form of this contribution, or allow others to do so, for U.S. Government purposes.

* Corresponding author at: Baltusrol Road, Knoxville, TN 27934-3707, United States. Tel.: +1 865 675 4532.
E-mail address: Wunderlich@CharterTN.net (B. Wunderlich).

0040-6031/$ – see front matter. Published by Elsevier B.V.
doi:10.1016/j.tca.2006.07.005

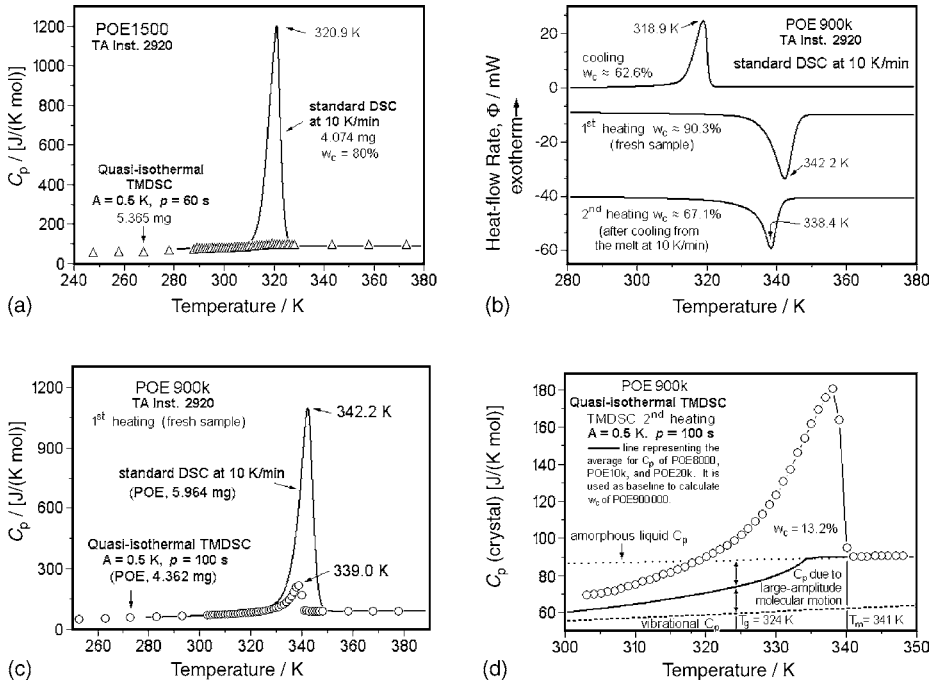

Fig. 1. Characteristic information on POE [24,16,17]. (a) Standard DSC trace of the melting of extended-chain crystals of low-molar-mass POE, showing an apparent C_p including the latent heat of fusion (melting peak), superimposed on the thermodynamic C_p from quasi-isothermal TMDSC. (b) Standard DSC traces at 10 K min^{-1} on cooling and heating. The heating traces were carried out with the as delivered, fresh samples (1st heating) and after the cooling-run from the melt (2nd heating). (c) Comparison of DSC and TMDSC of the as delivered sample. (d) Apparent reversing C_p of a high-molar-mass POE extrapolated to 100% crystallinity, and separated into thermodynamic C_p (heavy line) and latent heat contributions. The thermodynamic C_p has the appearance of a glass transition.

period. The term "reversible" is used only when the observed heat-flow rates on quasi-isothermal measurement are constant over long times, indicating that all irreversible changes have decayed to zero and the sample is metastable. Waiting times of more than 1 h were required only within the reversing melting peak. In the presently analyzed samples, a reversible latent heat of melting was indicated whenever a reversing C_p larger than the thermodynamic C_p was observed. The reversing melting of lower molar mass POE was studied earlier with temperature-modulated differential scanning calorimetry, TMDSC [16,24–27]. The extended-chain crystals of low molar mass have a structure that is close to equilibrium and shows no reversible melting, while the folded-chain crystals with relative high molar mass show some locally reversible melting, which depends on crystallization conditions and molar mass [16].

In the present research, the reversing melting and crystallization of a POE with an average molar mass of 900,000 Da, POE900k, is studied with quasi-isothermal TMDSC with changing amplitude in the melting range to gain information on the change of reversibility. Relevant earlier data are summarized in Fig. 1. First, in Fig. 1a, the irreversible melting of extended-chain crystals of ≈1500 Da is documented [24]. The irreversible fusion is seen from the total C_p by standard differential scanning calorimetry, DSC. The thermodynamic C_p without melting contributions, by the reversing C_p from quasi-isothermal TMDSC (Δ) which contains for this sample practically no latent heat contribution. The heat-flow rates by standard DSC for POE900k on cooling and for heating after two different crystallization histories are compared in Fig. 1b [17]. The listed crystallinities are estimated from the heat-flow rates relative to a suitable straight baseline. Fig. 1c illustrates the total, apparent C_p as gained from the standard DSC, and the quasi-isothermal, apparent, reversing C_p (◯). The vibrational C_p of the crystals of PEO and the contribution to C_p caused by large-amplitude motion are shown in Fig. 1d together with the quasi-isothermal, apparent, reversing C_p on second heating. The sum of the vibrational and large-amplitude C_p is the thermodynamic C_p marked by the heavy line [18]. Its increase is interpreted as the T_g of the crystal at the temperature of half-increase. This observation is based on a thermodynamic description of crystallization consisting of an ordering and a glass transition [17,18].

2. Experimental

2.1. Material

The poly(oxyethylene), POE900k, used in this research had a viscosity-average molar mass, M_v, of ≈900,000 Da and was purchased from Aldrich Chemical Co. It is a white powder of density d = 1.210 Mg m^{-3} and with a crystallinity of approximately 90%. On cooling from the melt at 10 K min^{-1}, this crystallinity decreases to about 70%. Decomposition was inhibited with 200–500 ppm BHT (butylated hydroxytoluene, 3,5-di-*tert*-butyl-4-hydroxytoluene), added by the manufacturer. The equilibrium melting temperature for this molar mass POE is taken to be 342 K [27], the glass transition temperature of the amorphous polymer was estimated to occur at 206 K [15], although it is broadened considerably due to crystallinity. The glass tran-

sition of the crystal, taken at the midpoint of the increase of C_p, is seen in Fig. 1d at 324 K [16,17].

2.2. Instrumentation and experimental details

The calorimetry was carried out with a Thermal Analyst 2920 system from TA Instruments, Inc. The calorimeter is of the isoperibol heat-flux, twin type, capable of standard DSC and quasi-isothermal temperature-modulated TMDSC. The temperature measurement and modulation control is by the sample-temperature sensor. During the experiments, a refrigerated cooling system with a cooling capability to 220 K, was used, and dry N_2 gas with a flow rate of 25 mL min^{-1} was purged through the DSC cell. The temperature was calibrated in the standard DSC mode, using the onset temperature of the melting-transition peak for indium at 429.75 K, and the heat-flow rate was pre-calibrated at a scanning rate of 10 K min^{-1} with the specific heat of fusion of indium of 28.62 J g^{-1} [28]. The melting temperature of indium was also measured in the quasi-isothermal TMDSC mode with a 0.5 K amplitude and 100 s period after calibration in the standard DSC mode, to identify any differences. It was found that quasi-isothermal TMDSC experiments after initial standard DSC calibration led to a melting temperature of 428.89 K. To correct the temperatures from the quasi-isothermal measurements, a constant of 0.86 K was added to the average temperatures of the quasi-isothermal measurements carried out at T_o.

In all the experiments, standard aluminum pans of 20 μL with covers were used for the sample and the empty reference. A somewhat lighter reference pan was used for all measurements to approximately correct for the asymmetry of the calorimeter [29]. The standard DSC was performed at 10 K min^{-1}. A fresh POE sample was used in all 1st heating runs.The quasi-isothermal TMDSC was carried out using sinusoidal modulation about successive base temperatures, T_o, with a modulation period of p = 100 s, and a modulation amplitude varying from 0.2 to 3.0 K. The quasi-isothermal runs were used to calculate the apparent, reversing C_p:

$$mc_p = \frac{A_\Phi}{A_{T_g}\omega} \times \sqrt{1+\tau^2\omega^2}, \quad (2)$$

where m is the sample mass; c_p, the specific heat capacity in J K^{-1} g^{-1}; A_Φ, the amplitude of the heat-flow rate; A_{T_s}, the amplitude of the temperature modulation; $A_{T_s}\omega$ is the amplitude of the heating rate for a sinusoidal modulation with frequency ω (=$2\pi/p$, where p is the period in s); and τ represents the calibration factor at the given conditions [30]. To measure the crystallinity of the sample, a standard DSC trace at 10 K min^{-1} was occasionally run immediately after the completion of the quasi-isothermal TMDSC. Unless otherwise stated, the crystallinity, w_c, shown in the figures was calculated from $w_c = (\Delta H(\text{measured})/\Delta H_f)$, where the heat of fusion of 100% crystalline POE is 196.6 J g^{-1} at the equilibrium melting temperature of the sample, T_m^0 = 342 K [22,23].

3. Results

3.1. The reversible melting of POE900k

Fig. 2 illustrates the quasi-isothermal TMDSC [17]. In Fig. 2a the apparent reversing C_p of Fig. 1c is amplified, and data for cooling and the second heating are added. In Fig. 2b, the long-time quasi-isothermal analyses are given at the three peak temperatures shown in Fig. 2a. The double exponential fit to the

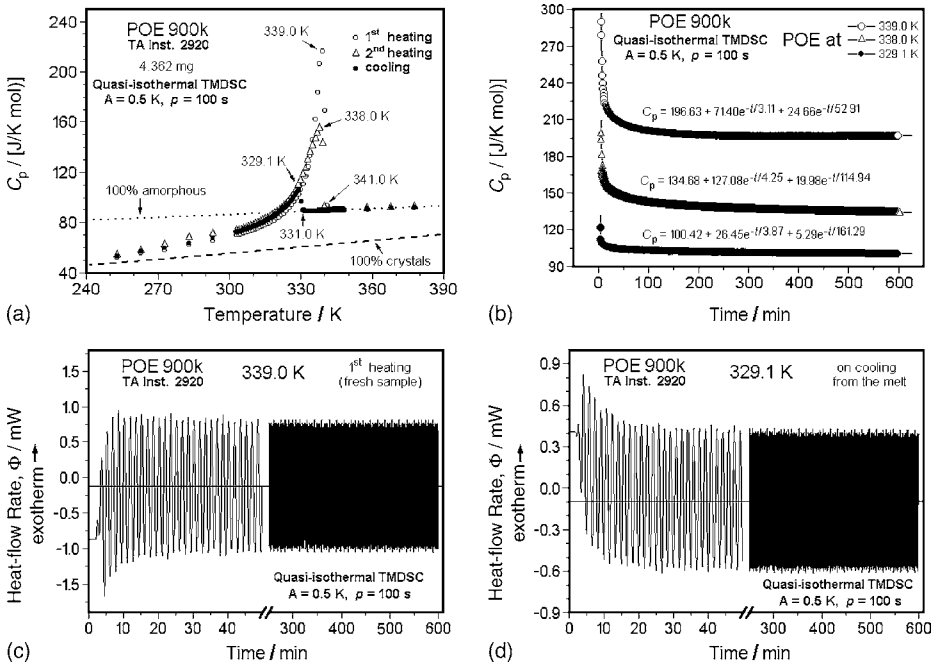

Fig. 2. Time dependence of the apparent reversing C_p of POE [17]. (a) Apparent reversing C_p of the samples of Fig. 1b. (b) Long-time quasi-isothermal analysis at the peak temperatures shown in (a). (c and d) Modulated heat-flow rates on quasi-isothermal analysis of melting on heating and crystallization on cooling.

curves yields the reversible $C_p s$ at infinite time. The decreasing reversing C_p does not reach the expected thermodynamic C_p, as mentioned above. For truly reversible melting, as is known in crystal-seeded indium, the range of reversibility could be proven by quasi-isothermal TMDSC to be narrower than ±0.05 K [31,32]. The short relaxation times in Fig. 2b are partly due to lags within the calorimeter and overlap with the irreversible melting and crystallization. The long relaxation times decrease with temperature and are linked to slow crystal perfection. Fig. 2c and d contain plots of the reversing heat-flow rates at the melting peak of 339.0 K and the crystallization peak at 329.1 K of Fig. 2a. At the start of the experiments, the modulated portion of the heat-flow rate is superimposed on the continuing irreversible melting (endotherm) or crystallization (exotherm). Initially the superimposed modulation is asymmetric, but approaches close to symmetric amplitudes within a few minutes. After about 5 min a meaningful reversing $C_p s$ can be calculated with Eq. (2). The major irreversible melting has decayed after about 15 min, while the crystallization continues to about 25 min, agreeing with the generally slower crystallization than melting. At the beginning of melting at 339 K in Fig. 2c, the endothermic reversing heat-flow rate is larger than the exothermic one. This excess in the endotherm decreases with time, while the exotherm exceeds its constant level for long times. At about 10 min into the experiment, a shallow maximum appears in the amplitude of the exotherm, connected to the reorganization or recrystallization of the crystals. Once the crystal portions produced by the local crystallization are improved beyond those of the melted parts, the next cycle of melting cannot melt them again, causing the decrease in C_p, described by the second relaxation time of Fig. 2b. Ultimately, the locally reversible melting process is reached beyond 300 min. In the cooling run at 329.1 K of Fig. 2d, close to similar exotherms and endotherms are reached more quickly and are superimposed on the slower irreversible crystallization.

3.2. Amplitude-dependence of the quasi-isothermal TMDSC

The effect of the modulation amplitude on the reversing, apparent C_p within the melting peak of the fresh sample was studied by a sequential measuring program as illustrated in Fig. 3. In Fig. 3a the change of the heat-flow amplitudes is illustrated for a molten sample, quickly cooled to 338.4 K. This is a temperature just below the maximum in reversing melting of the fresh sample on heating. The sample was then analyzed in each of nine steps with modulation amplitudes of 0.2–3.0 K and back to 0.2 K. Crystallization begins only below 331 K, as was found earlier on the same PEO900k by cooling from the melt as illustrated in Fig. 2a [17]. Since in this experiment there is no latent heat effect, one can see in Fig. 3a a quick attainment of steady state for all modulation amplitudes and the overall reversing heat capacity of the sample in Fig. 3b is constant and identical for all amplitudes, as expected. This information is used as baseline for the discussion of the reversing melting of the crystallized sample of Fig. 3c and d.

In Fig. 3c and d a fresh sample of PEO900k of initially 90.3% crystallinity is analyzed by a series of 20 min modulation with an amplitude of 0.5 K up to 337.9 K with results similar to the data shown in Fig. 2a. This is followed by the experiment at

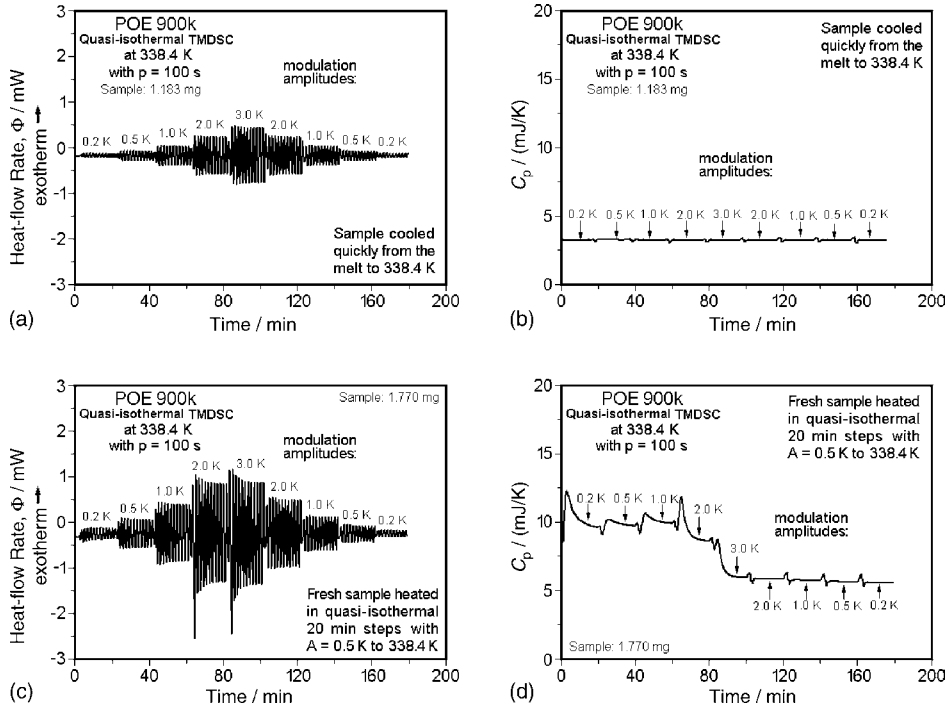

Fig. 3. Modulated heat-flow rates and reversing C_p of PEO900k as a function of time. (a and b) After cooling from the melt to a base-temperature T_o of 338.4 K and different modulation amplitudes (p = 100 s). (c and d) The same experiment after heating a fresh sample quasi-isothermally with an amplitude of 0.5 K to T_o = 338.4 K (see Fig. 2a).

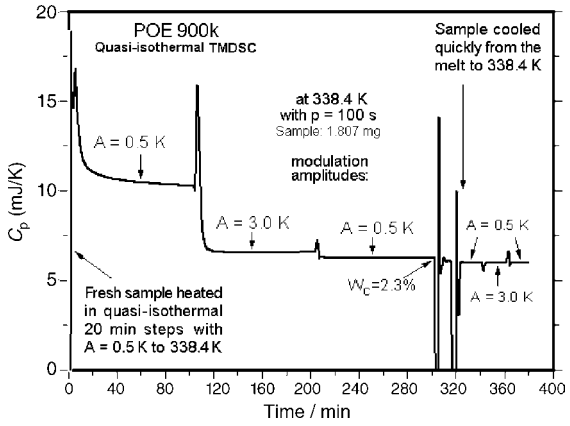

Fig. 4. Reversing C_p of PEO900k as a function of time. Repeat run of Fig. 3d at 338.4 K with long-time modulation and amplitudes of 0.5 and 3.0 K, followed by DSC to the melt and quick cooling to 338.4 K for the determination of the reference C_p.

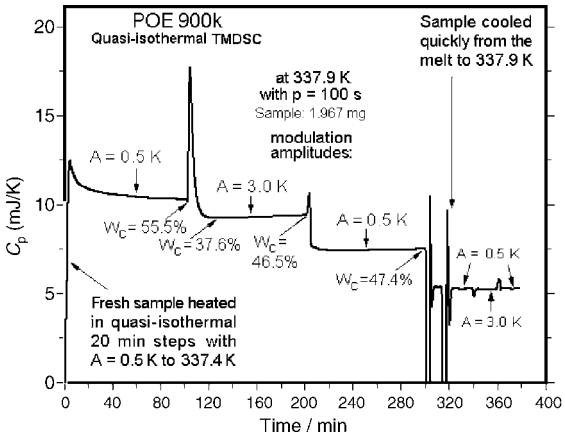

Fig. 5. Reversing C_p of PEO900k as a function of time. Repeat run of Fig. 4 at 337.9 K with long-time modulation and amplitudes of 0.5 and 3.0 K, followed by DSC to the melt and quick cooling to 337.9 K for the determination of the reference C_p.

338.4 K, starting at the time 0 of Fig. 3c. The corresponding reversing heat capacity is displayed in Fig. 3d. There is a larger response than expected from the thermodynamic heat capacity of a semicrystalline sample. Steady state is not reached in the 20 min time periods for each amplitude. Major amounts of irreversible melting can be seen for the amplitudes 2.0 and 3.0 K, and less reversing melting is obvious after the 3.0 K modulation. In the last four steps, the heat capacity approaches that of Fig. 3b (after normalizing to equal masses). At time zero, the crystallinity can be estimated from the standard DSC in Fig. 1b to be 63%, as is illustrated in more detail in Fig. 8d, below.

Analogous experiments were carried out at higher temperatures to ascertain the end of melting from experiments at base temperatures of T_o = 338.9, 339.4, and 340.4 K. In these three experiments, practically no melting was observed beyond the 3.0 K amplitude. The data will be discussed in Section 4.2 with Fig. 7.

In order to increase the accuracy of the experiments at higher temperatures, and also all subsequent measurements with longer modulation sequences, the reference runs were made immediately after the melting sequence without removing the sample from the calorimeter. After the initial quasi-isothermal analysis, the sample was heated by standard DSC to complete the melting and to gain information on crystallinity. Next, the melted sample was cooled to the earlier T_o for a reference sequence as was carried out before in a separate run. From the experiments on cooling, one expects no crystallization above 331 K.

In Fig. 4, the modulation sequences at 338.4 K are extended to 100 min for amplitudes of 0.5, 3.0, and 0.5 K, followed by complete melting and determination of a baseline. The remaining crystallinity at 300 min is only 2.3%. Fig. 5 represents the results of identical experiments carried out at a temperature lower by 0.5 K. The changing crystallinities are marked in the figure. They were derived from separate experiments. After the last modulation, the crystallinity is 20 times higher than at 338.4 K. As in Figs. 4 and 3d, the initial endothermic spikes in the apparent reversing heat capacity are indicating the irreversible melting. During the spike, the apparent, reversing C_p is not properly deconvoluted from the total C_p because of nonstationarity. The slow increases in reversing C_p is connected to an increase in crystallinity of the runs at 3.0 and subsequent 0.5 K amplitude. Such an increase in C_p is also seen for 338.4 K, but to a lesser degree.

4. Discussion

4.1. Analysis of the components of the modulated heat-flow rates in Fig. 3

For a more detailed analysis of the melting behavior seen in Figs. 3–5, expanded heat-flow-rate curves were computed. The last 5 min of the measured heat-flow rates of the reference experiment, gained by cooling from the melt to the given temperature, were subtracted from heat-flow rates of the fresh, semicrystalline samples which approached the same temperature by heating. The phase-shifts of the heat-flow rates were small, as can be seen from the shift in maxima and minima for the experiments with larger modulation amplitudes. The resulting difference in heat-flow rate, $\Delta\Phi$, allows a discussion of the reversing melting.

The heat-flow-rate obtained after cooling from the melt is drawn in Figs. 6a–d and 7a as the solid line in the bottom portions of the graphs. The amplitudes increase linearly with increasing modulation, as expected. The amplitudes of the semicrystalline samples are superimposed as dashed lines. They include the latent heats of the reversible melting. The heat capacities of the amorphous and crystalline phases are practically identical in this temperature region (see Fig. 1d). As a result, the curves of $\Delta\Phi$ should give a measure of the latent heat during modulation. Checking the symmetry of the modulation due to the latent heat relative to time, one observes for all five curves that the exothermic maximum is shifted by 2.5 ± 1.1 s to earlier times relative to the time expected from the average of the adjacent exothermic minima, a finding which will be discussed further in Section 4.3. The reference curve after cooling from the melt is strictly symmetric, as can be checked by flipping

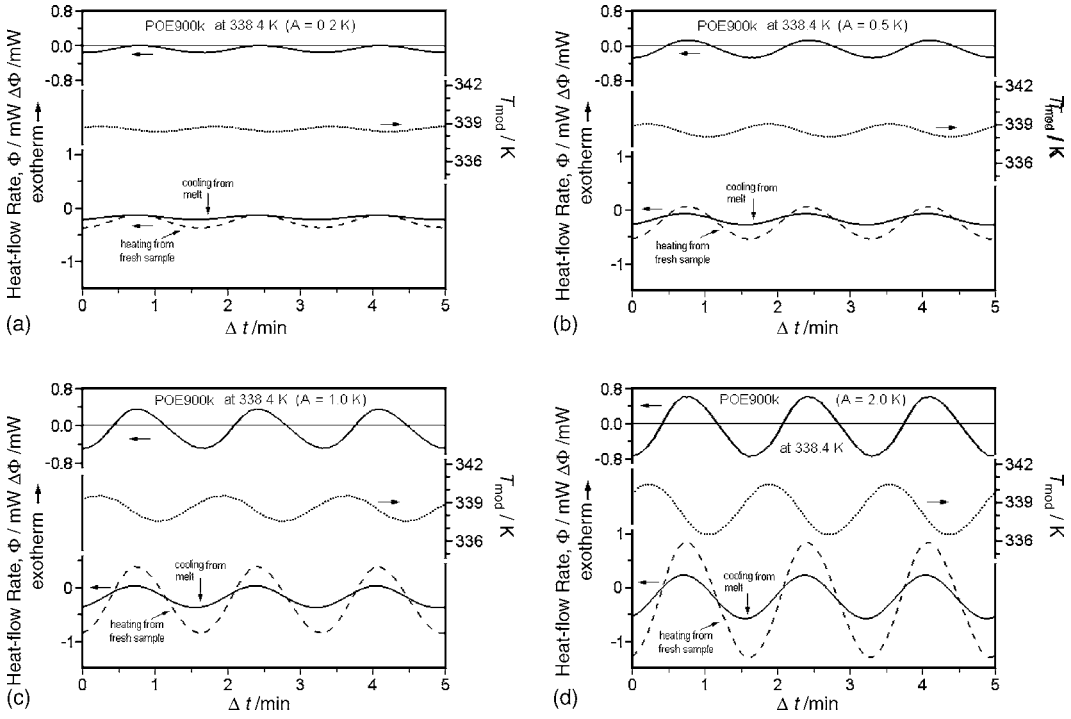

Fig. 6. Analysis of the heat-flow rates during the last 5 min of the first four modulation sequences in Fig. 3. Shown are the modulated temperatures in the center traces, the heat flow rates of the semicrystalline sample from Fig. 3c and the reference in Fig. 3a as the bottom traces, and their heat-flow rate difference $\Delta\Phi$ as the top traces.

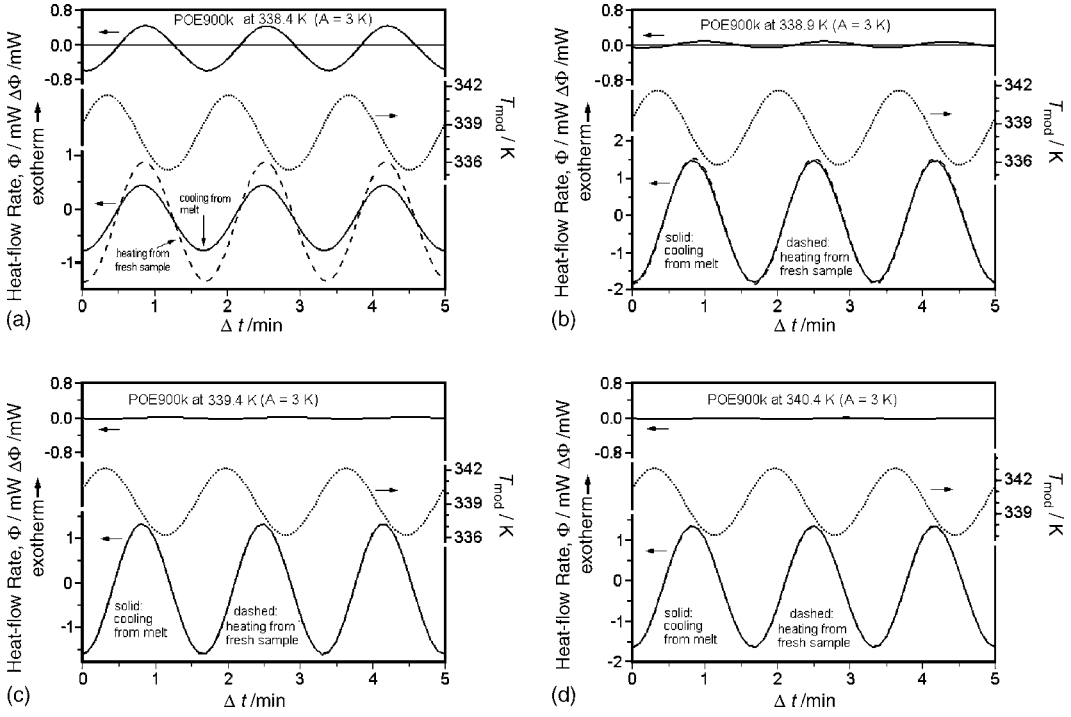

Fig. 7. (a) Analysis of the heat-flow rates during the last 5 min of the fourth modulation sequences in Fig. 3. Shown are the modulated temperatures in the center trace, the heat flow rates of the semicrystalline sample from Fig. 3c and the reference in Fig. 3a as the bottom traces, and their heat-flow rate difference $\Delta\Phi$ as the top trace. (b–d) Analogous runs, modulated at 338.9, 339.4, and 340.4 K with sample masses of 3.148, 3,313, and 3.134 mg, respectively. All runs are at amplitudes of 3.0 K.

the curves about a vertical axis and superimposition. The corresponding apparent heat capacities in Fig. 3 were computed from Eq. (2), making use of the dotted temperature amplitudes in the center and the dashed heat-flow-rate amplitudes. Their magnitudes are discussed in Section 4.4. The phase-shifts between the different heat-flow rates could also be used to deduce thermal effects, but are more difficult to properly calibrate [34,35].

In Fig. 6a, the experiment with the smallest amplitude of temperature modulation, an unmodulated (irreversible) shift is seen in the endothermic direction of $\Delta\Phi$. This small endotherm is constant and has the same magnitude for the other four amplitudes of Fig. 3, displayed in Figs. 6b–d and 7a (average: $60.9 \pm 7\,\mathrm{mW\,g^{-1}}$, sample mass 1.183 mg). The heat-flow rate per unit mass is larger than could originate from the continuing irreversible melting. In Fig. 2c a sample of 4.362 mg at 339 K was analyzed. In this experiment the irreversible melting has already decreased after 10 min from its initial value of 160 to 23 $\mathrm{mW\,g^{-1}}$ and decreases exponentially at longer times. Furthermore, the later comparisons in Figs. 7–9 where done by calibrations without removal of the sample from the calorimeter and showed no endothermic deviation in $\Delta\Phi$. Based on these observations, one must assume that the small, constant endotherm in $\Delta\Phi$ is a systematic error caused by the separate run for the baseline with different sample, pan, and placement of the pan. Similar constant changes in the asymmetry of the heat-flow rates have been observed in the past when pans were deformed during the experiment [33].

4.2. Analysis of the end of melting

Next, Fig. 7 provides a comparison for the 3.0 K modulations at four increasing base temperatures, T_o. The last sizeable reversible melting occurs at $T_o = 338.4$ K (Fig. 7a). Its modulation reaches up to 341.2 K. In Fig. 7b–d only negligible reversible latent heat is left. At 338.9 K, the modulation reaches up to 341.6 K, and at 339.4 and 340.4 K to 342.1 and 343.1 K, respectively. These temperatures are in agreement with the equilibrium melting temperature for the PEO900k at 342.0 K [27]. A remaining uncertainty of, perhaps, 1 K can be accounted for by a small amount of the sample in the center of the pan which may retain a somewhat lower temperature than indicated by the external thermocouple. Such internal temperature gradients are expected in quasi-isothermal TMDSC and were documented by external, contact-less infrared thermography from outside the calorimeter [36]. It was shown in Ref. [36] that the upper surface of the aluminum pan follows the temperature of the bottom surface without a significant lag. The lower thermal conductivity of the sample, however, causes gradients which make the interior of the aluminum-encased sample have a decreased modulation-amplitude.

4.3. Analysis of the components of the modulated heat-flow rates in Fig. 4

In Fig. 8a–c comparisons of heat-flow amplitudes are given for the long-time experiment of Fig. 4. Fig. 8a and c illustrate

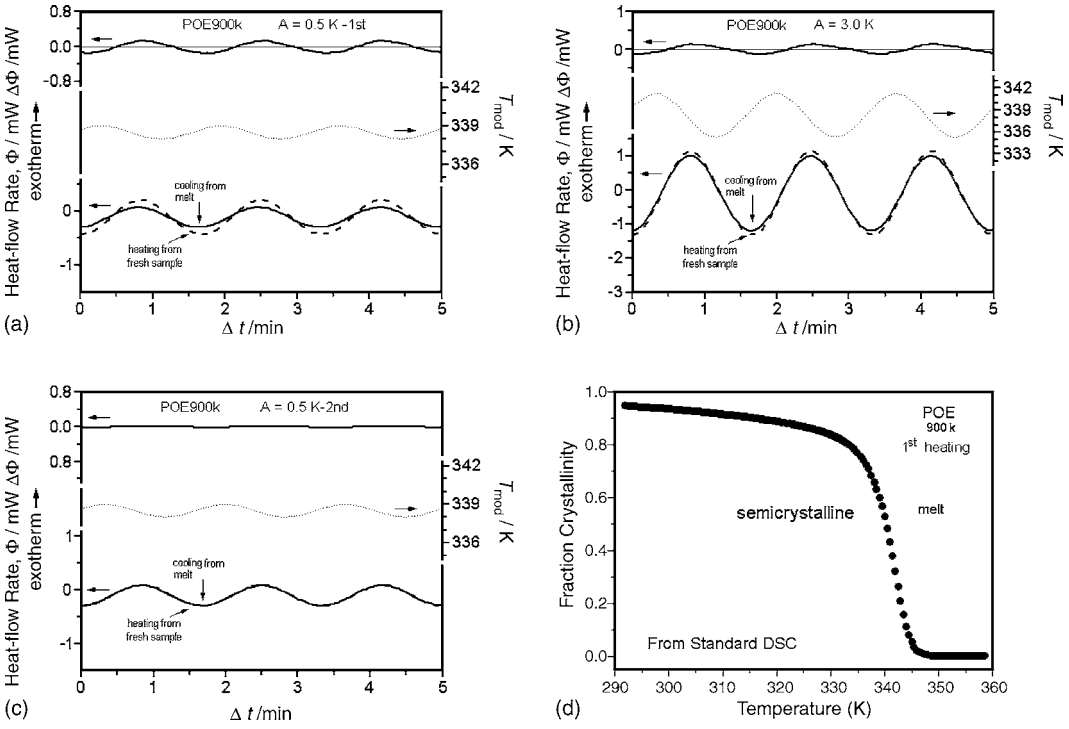

Fig. 8. (a–c) Analysis of the heat-flow rates during the last 5 min of the first three modulation sequences in Fig. 4. Shown are the modulated temperatures in the center traces, the heat flow rates of the semicrystalline sample and the reference in Fig. 4 as the bottom traces, and their heat-flow rate difference $\Delta\Phi$ as the top traces. (d) Fractional crystallinity as determined from standard DSC on heating of the fresh sample at 10 K $\mathrm{min^{-1}}$ considering the temperature-dependence of the heat of fusion (compare also to Fig. 1b).

the difference of the sample of high and low crystallinity, both modulated with an amplitude of 0.5 K. The differential heat-flow rates are symmetric to the zero line. In Fig. 8a the sample should still have a crystallinity of close to the 60% as estimated for the analysis given in Fig. 8d. The two differential maximum amplitudes of $\Delta\Phi$ derived from Figs. 8a and 6b are similar (90 and 116 mW g^{-1}, respectively), and the shift of the exothermic maximum to earlier times is also of the same magnitude. By 300 min into the experiment, the time of the end of the second 0.5 K modulation, the crystallinity has dropped to 2.3% and, accordingly, the amplitude in Fig. 8c is practically zero. The $\Delta\Phi$ at the 3.0 K amplitude in Fig. 8b is about the same as in Fig. 8a (maximum of 80 mW g^{-1}), but should be much bigger because of the higher modulation amplitude. Fig. 4 suggests, that this decrease is due to a drop in crystallinity, indicated by the strong endothermic spike in the C_p curve at the beginning of the 3.0 K modulation. A comparison with the change in crystallinity on measurement by standard DSC is illustrated in Fig. 8d. This figure was calculated using the proper heat capacity baseline and considering the change of heat of fusion with temperature [17]. Further discussion of the reversibility is given in Section 4.5.

4.4. Analysis of the components of the modulated heat-flow rates in Fig. 5

In Fig. 9, the same comparison of heat-flow amplitudes as in Section 4.3 is given for a temperature lower by 0.5 K, based on the long-time experiment of Fig. 5. The crystallinity of this sample at time zero is estimated from Fig. 8d to be 67%. With the lower T_o, a more gradual change in crystallinity is reached. In addition, the experiment was repeated several times for different lengths of time to evaluate the crystallinities. Fig. 9a and c illustrate the difference of identical temperature modulation at different crystallinities. The differential heat-flow rates are symmetric about the amplitude zero, and the two maxima are 319 and 186 mW g^{-1} when normalized to 100% crystallinity and unit temperature modulation. The normalized maximum in $\Delta\Phi$ in Fig. 9b is much larger (315 mW g^{-1}).

The difference in length of the two half-cycles of $\Delta\Phi$ in Fig. 9b is now obvious. The crystallization half-cycle reaches its maximum about 5 s earlier than expected from a sinusoidal response. The inset in Fig. 9b was generated by parsing the indicated quarter of heat-flow-rate response beyond the melting peak (REF) and generation a full reference curve. The parsed section is expected to be closest to equilibrium because of the usually faster melting than crystallization. The shaded area created by the overlaid reference curve shows that the crystallization slows as the temperature decreases from T_o and continues with an exothermic contribution up to melting peak. In this way, the overall integral of the heat-flow rate over one period stays practically constant. With these analyses, it is shown that TMDSC has the potential of supplying more detail about reversible melting. Although the heat capacity analysis in Section 4.5 gives more quantitative data, it needs the heat-flow rate data to assess the asymmetries.

4.5. Analysis of the specific reversible heat capacities

The three sets of modulation experiments, which are displayed in Figs. 3–5, were carried out to obtain information about

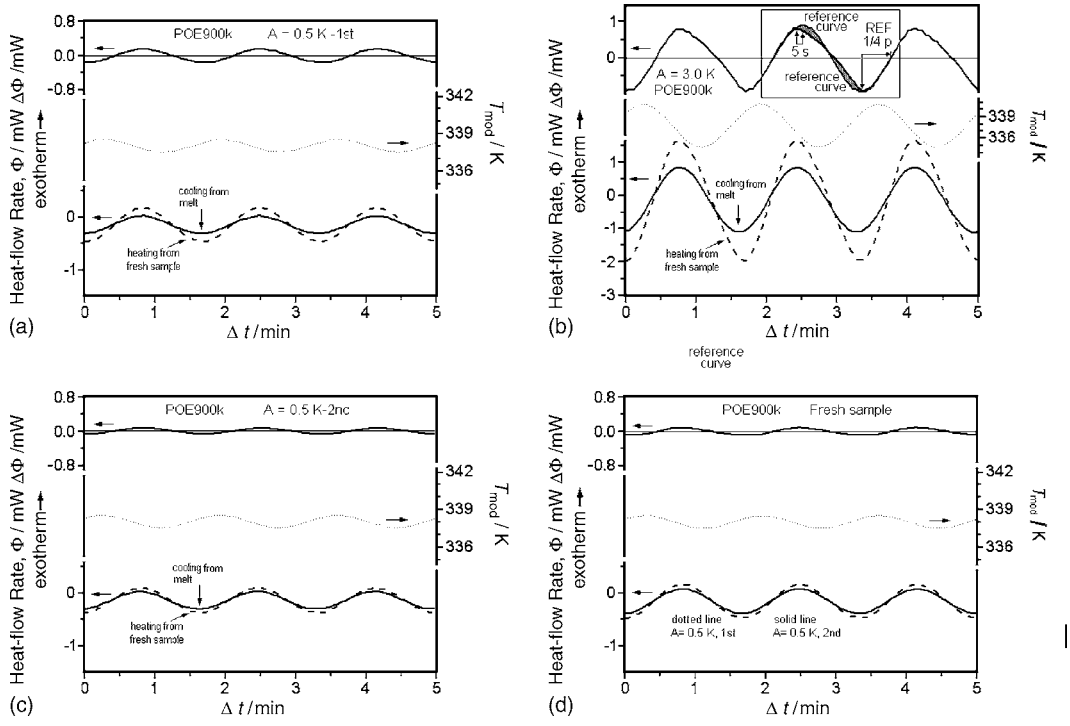

Fig. 9. (a–c) Analysis of the heat-flow rates during the last 5 min of the first three modulation sequences in Fig. 5. Shown are the modulated temperatures in the center traces, the heat flow rates of the semicrystalline sample and the reference in Fig. 5 as the bottom traces, and heat-flow rate differences $\Delta\Phi$ as top traces. The inset in (b) displays a superposition of a reference curve from the indicated parsed segment of 1/4*p*. (d) Difference of the of the two 0.5 K modulations.

the change in specific reversibility at the end of melting. The specific reversibility is given by the percentage of the reversible melting relative to the total melting (the loss of crystallinity on heating by 1 K at the same average temperature) [37]. The total melting should be measured by a comparable standard DSC measurement, which, however, suffers in the melting range from an increasing instrument lag [38]. A method which resolves this problem in a single measurement is a temperature modulation in the sawtooth mode with sufficiently long periods so that the standard DSC and reversible TMDSC can be evaluated from the same measurement [39]. In the present experiment, a similar method was used by combining sinusoidal modulation with a separate standard DSC trace. The total melting contributes also to the endothermic spikes in the jump to the first modulation cycle at higher temperature, T_o, or of larger amplitude, A. Separation from instrument effects, continued melting, and reorganization, however, makes this simultaneous evaluation difficult, so that spikes were only used as qualitative indicators for the irreversible decrease in crystallinity.

The apparent heat capacities for the time period close to reversibility were then converted first to reversible latent heats per kelvin of temperature change by subtracting the appropriate heat capacity of the melt, either from separate calibration runs or by consecutive calibration after melting and cooling of the same sample to the temperature of analysis. The resulting reversible latent heat is then converted into the change of crystallinity (in per cent) by division with 1.966 J g^{-1}, the latent heat to melt 1% of crystallinity close to T_m^o (see Eq. (1)).

Comparing the crystallinity of 55.5% of Fig. 5 with the data of Fig. 8d by standard DSC, one can conclude that up to 338.4 K there is only little temperature lag in the latter. The 0.5 K modulation reaches up to 338.4 K for which Fig. 8d registers a crystallinity of 62.8%, a value which is reasonable for time zero in Fig. 5. The slope of the crystallinity curve of Fig. 8d changes from 2% K^{-1} (at 80% crystallinity or 333.4 K), to 4.5% K^{-1} (70% or 337.1 K) and 8.5% K^{-1} (60–40% or 340.4–341.4 K). This also compares well with the change of crystallinity in Fig. 5 across the tallest melting peak which causes a change in the crystallinity of (55.5–37.6) = 17.9% for a change in maximum temperature of 2.5 K (for a slope of 7.2% K^{-1}). With the data of Fig. 5 at the time of 100 min, the specific reversibility for the 0.5 K modulation is 18%. Using the higher slope of 8.5% K^{-1} for the 3.0 K modulation at 125 and 200 min, the specific reversibility is decreased to 12 and 12.7%, respectively. At 215–300 min, on decreasing the modulation amplitude back to 0.5 K, the specific reversibility reduces further to 7%. An estimate of the error in these data can be gained by assuming a linear change in crystallinity from 337.9 K, where the lag is still small, to the end of melting at 341 K (see Fig. 2a). This results in a slope of 15% K^{-1}, so that the last three specific reversibilities may be only half the quoted values because of the lag of the standard DSC experiment.

The reduction of the specific reversibility between the two 0.5 K modulation sequences by more than the decrease in crystallinity is in accord with the connection of the reversible melting to molecular nucleation [40] as first suggested on the discovery of reversible melting on the example of poly(ethylene terephthalate) [41]. By melting of chain segments at the surface without losing the molecular nucleus, reversibility finds a simple explanation. The intermediate raising of the amplitude of modulation, causes further melting and a loss of the less stable molecular nuclei. Such different melting temperatures for different segments of high molar mass polymer molecules were earlier proven directly for polyethylene by fractionation after partial melting [42]. One assumes that the higher melting segment of the same molecule provides the molecular nucleus for the lower melting segment, which can now melt reversibly until the higher melting segment is removed with a higher modulation amplitude. There is no easy explanation for reversible melting when invoking an intermediate, less-ordered phase, as has been speculated to occur on crystallization [43].

The increase in crystallinity by 8.9% over the 80 min of 3.0 K modulation between the measurements in Fig. 5 cannot be exclusively linked to the slow crystallization seen in the inset of Fig. 9b. The slow crystallization accounts for about 15% of the integrated differential heat-flow rate of one cycle, while the total reversibility corresponds to a crystallinity change by ±3.2%, i.e., the 48 cycles would produce three times as much of an increase of crystallinity. This more detailed analysis of the asymmetry between melting and crystallization suggest that besides the main, fully reversible part of melting and crystallization, there is a slower crystallizing fraction. The earlier observed Lissajous ellipses were almost symmetric [17], but based on the construction in Fig. 9b one must conclude now that some of the melting is reversing and not reversible, i.e., shows different melting and crystallization temperatures. Since this slower crystallization stretches into the temperature region of melting, one might expect that part of this crystallization at higher temperature leads to higher crystal perfection and may cause the slow increase in crystallinity, lasting in the case of the 3.0 K modulation beyond 100 min.

Earlier approximations of the specific reversibility were reported for folded-chain crystals of high-density polyethylene [44]. Between 280 and 350 K, the specific reversibility ranged from 50–75%, decreasing toward zero when approaching the end of melting. For linear-low-density polyethylenes of about 30 wt.-% 1-octene, the specific reversibility between 250 and 300 K reached a maximum close to 90% [44], again, decreasing toward zero at higher temperatures. Extended-chain polyethylene [45], POE [16], and also low-molar-mass POEs grown into folded crystals [17], in contrast, show close to 0% specific reversibility, as seen in Fig. 1a [24], i.e., such samples show no locally reversible melting. The limit of 100% specific reversible melting of normal paraffins and short-chain polyoxides was also established by TMDSC. It occurs at about 75 chain atoms [26], much shorter than the limit of chain folding at about 250 chain atoms which was established by studies of the morphology [46,47]. In this paper the approach to the final melting of the high-molar-mass, folded-chain POE is shown for the first time to reach small values of specific reversibility, but does not go to zero. Even the highest temperatures in Fig. 7 illustrate still traces of reversibility, although the true sample temperature may lag somewhat in temperature, as discussed in Section 4.2.

Looking back to Fig. 4, referring to 0.5 K modulation with correspondingly lower crystallinities than in Fig. 5, the specific reversibility, using the 8.5% K^{-1} for the 0.5 K modulation at 100 min, yields a value of 14% in good accord with Fig. 5. For the 0.5 K modulation at 300 min, the reversible latent heat is 0.16 J K^{-1} g^{-1}, corresponding to less than 0.1% of crystallinity. Assuming all of the remaining 2.3% crystallinity melts on heating by one more kelvin, the specific reversibility would reach 3.5%. Using the same slope for the 3.0 K modulation, a reversibility of 8.2% is obtained. The lower increase in crystallinity with modulation time in Fig. 4 is simply due to the lesser remaining crystallinity than in Fig. 5. Fig. 3, finally shows no increase in crystallinity with time, the initially larger endotherm seen in Fig. 2c is not decayed sufficiently to see the effect of the annealing exotherm with the longer relaxation time. Estimating the specific reversibility of the initial modulation sequences of 0.2, 0.5, 1.0, and 2.0 K with the 8.5% K^{-1} slope of Fig. 8d, yields 16, 16, 17, 13%. The remaining modulations give reversible latent heats of the same magnitude as the 3.0 and 0.5 K modulations in Fig. 4. Because of the less-accurate calibration, discussed in Section 4.1, no quantitative comparison can be given for the small amplitudes.

5. Conclusions

In this research quasi-isothermal TMDSC is explored for the quantitative analysis of the reversible melting of POE of high molar mass (Figs. 6–9). Calibration methods were developed to assess reversible crystallinities as small as 0.08%. A latent heat of 0.16 J K^{-1} g^{-1} in a 1.8 mg sample was measured in the presence of a heat capacity of 3.3 J K^{-1} g^{-1} of the overall sample, and separated from a total, irreversible heat of fusion of 123.5 J g^{-1} during the overall experiment in Fig. 4. The melting end is explored with Fig. 7 and points to the possibility to also study the crystal-melt distribution within the sample pan during TMDSC. The earlier experiments, as summarized in Figs. 1 and d and 2, established reversing melting for crystals of high molar-mass POEs, a glass transition temperature lower than the irreversible melting peaks, and typical relaxation times for the crystal perfection [16,17]. Based on these results, the present measurements allow for the first time to quantitatively study the melt end of a polymer as displayed in Figs. 3–5. It was observed that the specific reversibility decreases as one approaches the melting end, but seems not to reach zero before completion of the irreversible melting. The distribution of the melting points of the reversibly melting species is broad and a small, characteristic fraction melts faster than it recrystallizes, i.e., it remains reversing under the chosen conditions. A quantitative separation of this fraction is possible with the analysis depicted in Fig. 9b. All observations point to the significance of the molecular nucleation process [40]. Because of the similarly observed reversible melting in many other semicrystalline, flexible macromolecules [48], TMDSC opens an opportunity of quantitative analysis of the crystal surface during melting and crystallization.

Acknowledgements

This work was supported by the Division of Materials Research, National Science Foundation, Polymers Program, Grant # DMR-0312233. Use of some of equipment and laboratory space was provided by the Division of Materials Sciences and Engineering, Office of Basic Energy Sciences, U.S. Department of Energy at Oak Ridge National Laboratory, managed and operated by UT-Battelle, LLC, for the U.S. Department of Energy, under contract number DOE-AC05-00OR22725.

References

[1] B. Lotz, A.J. Kovacs, G.A. Bassett, A. Keller, Kolloid-Z. Z. Polymere 209 (1966) 115.
[2] A.J. Kovacs, A. Gonthier, Kolloid-Z. Z. Polymere 250 (1972) 530.
[3] C.P. Buckley, A.J. Kovacs, Prog. Colloid Polym. Sci. 58 (1975) 44.
[4] A.J. Kovacs, A. Gonthier, C. Straupe, J. Polym. Sci. Polym. Symposium 50 (1975) 283.
[5] C.P. Buckley, A.J. Kovacs, Colloid Polym. Sci. 254 (1976) 695.
[6] A.J. Kovacs, C. Straupe, A. Gonthier, J. Polym. Sci. Polym. Symposium 59 (1977) 31.
[7] A.J. Kovacs, C. Straupe, J. Cryst. Growth 48 (1980) 210.
[8] S.Z.D. Cheng, B. Wunderlich, Macromolecules 22 (1989) 1866.
[9] S.Z.D. Cheng, A.Q. Zhang, J.S. Barley, J.H. Chen, A. Habenschuss, P.R. Zschack, Macromolecules 24 (1991) 3937.
[10] S.Z.D. Cheng, A.Q. Zhang, J.H. Chen, D.P. Heberer, J. Polym. Sci. Polym. Phys. 29 (1991) 287.
[11] S.Z.D. Cheng, J.H. Chen, J. Polym. Sci. Polym. Phys. 29 (1991) 311.
[12] S.Z.D. Cheng, J.H. Chen, A.Q. Zhang, D.P. Heberer, J. Polym. Sci. Polym. Phys. 29 (1991) 299.
[13] S.Z.D. Cheng, J.H. Chen, A.Q. Zhang, D.P. Heberer, Polymer 33 (1992) 1140.
[14] S.Z.D. Cheng, J.H. Chen, J.S. Barley, A.Q. Zhang, A. Habenschuss, P.R. Zschack, Macromolecules 25 (1992) 1453.
[15] H. Suzuki, J. Grebowicz, B. Wunderlich, Makromol. Chem. 189 (1985) 1109.
[16] W.L. Qiu, M. Pyda, E. Nowak-Pyda, A. Habenschuss, B. Wunderlich, Macromolecules 38 (2005) 8454.
[17] W. Qiu, M. Pyda, E. Nowak-Pyda, A. Habenschuss, B. Wunderlich, J. Polym. Sci., Part B: Polymer Phys., in press.
[18] B. Wunderlich, The glass transition of polymer crystals, Thermochim. Acta 446 (2006) 128.
[19] B. Wunderlich, Macromolecular Physics, Crystal Melting, vol. 3, Academic Press, New York, 1980.
[20] (a) U. Gaur, B. Wunderlich, J. Phys. Chem. Ref. Data 10 (1981) 1001;
(b) M. Varma-Nair, B. Wunderlich, J. Phys. Chem. Ref. Data 20 (1991) 349.
[21] J. Grebowicz, H. Suzuki, B. Wunderlich, Polymer 26 (1985) 561.
[22] B. Wunderlich, in: S.Z.D. Cheng (Ed.), Handbook of Thermal Analysis Calorimetry, vol. 3, Elsevier, Amsterdam, 2002, p. 1.
[23] For data see: http://web.utk.edu/~athas/databank.
[24] K. Ishikiriyama, B. Wunderlich, Macromolecules 30 (1997) 4126.
[25] K. Ishikiriyama, B. Wunderlich, J. Polym. Sci. Polym. Phys. 35 (1997) 1877.
[26] J. Pak, M. Pyda, B. Wunderlich, Thermochim. Acta 396 (2003) 43.
[27] Extrapolated for the extended-chain crystal of the appropriate molar mass using Figure VIII. 15 of Ref. [19].
[28] S.M.E. Gmelin, G.W.H. Höhne, H.K. Cammenga, W. Hemminger, W. Eysel, Thermochim. Acta 247 (1994) 129.
[29] K. Ishikiriyama, B. Wunderlich, J. Thermal Anal. 50 (1994) 337.
[30] R. Androsch, I. Moon, S. Kreitmeier, B. Wunderlich, Thermochim. Acta 357/358 (2000) 267.
[31] K. Ishikiriyama, A. Boller, B. Wunderlich, J. Thermal Anal. 50 (1997) 547.

[32] R. Androsch, B. Wunderlich, Thermochim. Acta 364 (2000) 181.
[33] J. Pak, W.L. Qiu, M. Pyda, E. Nowak-Pyda, B. Wunderlich, J. Thermal Anal. Calorim. 82 (2005) 565.
[34] A. Boller, Y. Jin, B. Wunderlich, J. Therm. Anal. 42 (1994) 307.
[35] B. Wunderlich, Y. Jin, A. Boller, Thermochim. Acta 238 (1994) 277.
[36] R. Androsch, M. Pyda, H. Wang, B. Wunderlich, J. Thermal Anal. Calorim. 61 (2000) 661.
[37] R. Androsch, B. Wunderlich, J. Polym. Sci., Part B: Polym. Phys. 41 (2003) 2039.
[38] B. Wunderlich, Thermal Analysis of Polymeric Materials, Springer, Berlin, 2005.
[39] W. Hu, B. Wunderlich, J. Thermal Anal. Calorim. 66 (2001) 677.
[40] B. Wunderlich, A. Mehta (Eds.), J. Polym. Sci., Polym. Phys. 12 (1974) 255.
[41] I. Okazaki, B. Wunderlich, Macromolecules 30 (1997) 1758.
[42] A. Mehta, B. Wunderlich, Makromolekul. Chem. 175 (1974) 977.
[43] G. Strobl, Acta Polym. 48 (1997) 562.
[44] R. Androsch, B. Wunderlich, J. Polym. Sci., Part B: Polym. Phys. 41 (2003) 2157.
[45] J. Pak, B. Wunderlich, J. Polym. Sci., Part B: Polym. Phys. 40 (2002) 2219.
[46] D.C. Bassett, R.H. Olley, S.J. Sutton, A.S. Vaughan, Macromolecules 29 (1996) 1852.
[47] D.C. Bassett, R.H. Olley, S.J. Sutton, A.S. Vaughan, Polymer 37 (1996) 4993.
[48] B. Wunderlich, Prog. Polym. Sci. 28 (2003) 383.